Chapter

Response of Coastal Upwelling East of Hainan Island in the South China Sea to Sudden Impact and Long-Term Variability of Atmospheric Forcing

Lingling Xie and Mingming Li

Abstract

The wind-driven coastal upwelling east of Hainan Island (UEH) in the northwestern South China Sea (SCS) is sensitive to the multi-scale variability of atmospheric forcing. This chapter focuses on two ends of time scales of atmospheric forcing: very short-time or sudden impact, i.e., typhoon passages; and long-term variability associated with El Niño events. The response of the sea surface temperature (SST) associated with the UEH to typhoon passages was investigated based on concurrent satellite SST and wind products. The long-term variability and response of the UEH to super El Niño events were analyzed based on recent 30 years of satellite data. The results show that the UEH has significant responses to atmospheric forcing. Meanwhile, the ocean circulation also plays an important role in modulation of the coastal upwelling.

Keywords: coastal upwelling, typhoon, ENSO, long-term variability, South China Sea

1. Introduction

As one of the important dynamic processes in continental shelf seas, coastal upwelling is capable of bringing the cold and nutrient-rich subsurface water to the surface [1–3]. Thus, it plays a crucial role in the local fishery [4, 5], sedimentation process [6, 7], and weather system [8, 9]. Meanwhile, the coastal upwelling is of significance for the air-sea CO_2 flux and the global carbon cycle [10, 11]. Hence, oceanographers have paid much attention to the coastal upwelling in various ocean areas [12–18].

The wind-forced offshore Ekman transport is the general mechanism for the coastal upwelling [16, 19–21]. In recent decades, with global climate change, the long-term and interannual variability of upwelling, particularly its response to extreme events, such as the El Niño-Southern Oscillation (ENSO) events, has been paid more and more attentions [22–27]. On the other hand, the coastal upwelling in low latitudes is susceptible to frequently passing tropical cyclones. The sudden impacts by typhoon passages on the upwelling process are worth pursuing [28–31].

As shown in **Figure 1**, upwelling east of Hainan Island (UEH) is seasonal coastal upwelling in the northwestern South China Sea (SCS). It occurs mostly within a

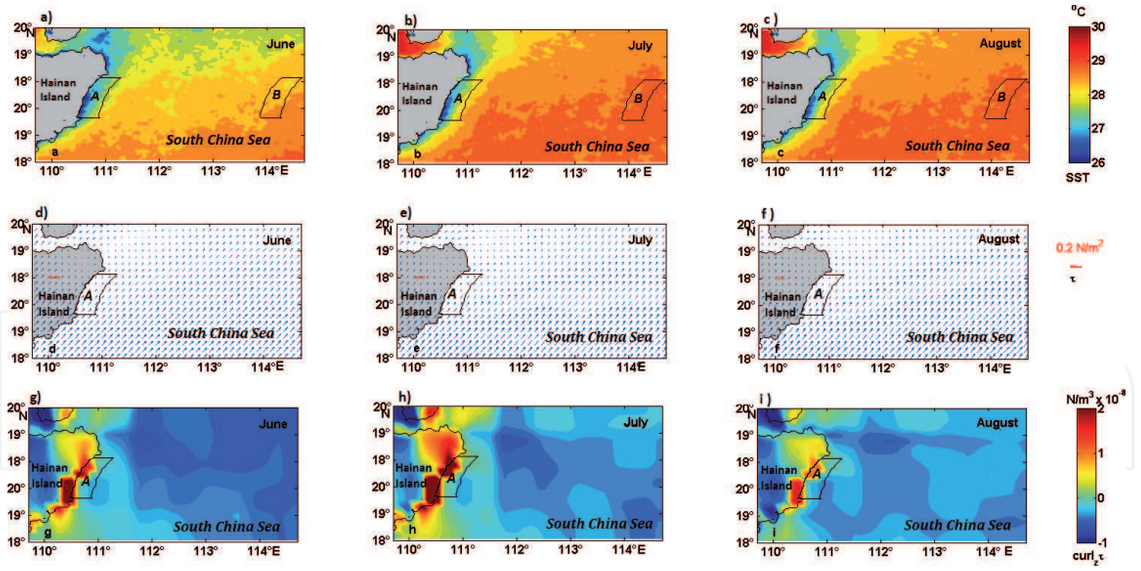

Figure 1.
Climatological monthly mean SST (a–c), wind stress vector (d–f), and wind stress curl (g–i) in summer months of June, July, and August in northern SCS. Black boxes A and B represent the coastal upwelling zone of the UEH and the background zone without upwelling in deep water, respectively.

range of 40 km off the coastline in summer months as the southwesterly monsoon prevails [16, 21, 32]. The wind-driven offshore Ekman transport and Ekman pumping, as well as the topography effect, are main mechanisms of the UEH [33–35]. Since pioneer studies in the 1960s, researchers have investigated the hydrographic features and the variability of the UEH [16, 31, 33, 36–39]. In recent years, the 3D vertical circulation and diapycnal turbulent mixing in the UEH zone have been investigated from cruise observations [21, 40].

2. Long-term variability of UEH

2.1 Climatology

As shown in **Figure 1a–c**, the SST reaches above 28°C in the most northern SCS. One can see that the low-temperature area along the eastern coast of Hainan Island formed by upwelling is quite evident with SST decreasing from 27.5°C at 40 km offshore to 26°C along the coast. In July and August, the SST reaches above 29°C in the deep water but is still lower than 27.5°C in the coastal upwelling zone. Influenced by East Asia monsoon, the southwesterly winds prevail in the northern SCS in summer as shown in **Figure 1d–f**. One can see that the wind stress in the offshore water east of Hainan Island is lower than that in the deep water. The winds blow northeastward over the offshore water. The non-zero wind stress curl is produced by nonuniform spatial distributions of wind speed and wind direction. From the wind stress curl shown in **Figure 1g–i**, one can see that in summer, the wind stress curl east of 112°E in the northern SCS is generally negative, while that over the coast upwelling zone between 110° and 111°E is positive in June–August, and the value and extent are larger in July. Driven by the positive wind stress curl, the Ekman pumping can cause upwelling of lower layer cold water, leading to the UEH with low SST.

2.2 Variability of upwelling intensity

We use the SST difference between the upwelling zone (Zone A in **Figure 1**) and that in the deep water without upwelling (Zone B in **Figure 1**) as the upwelling

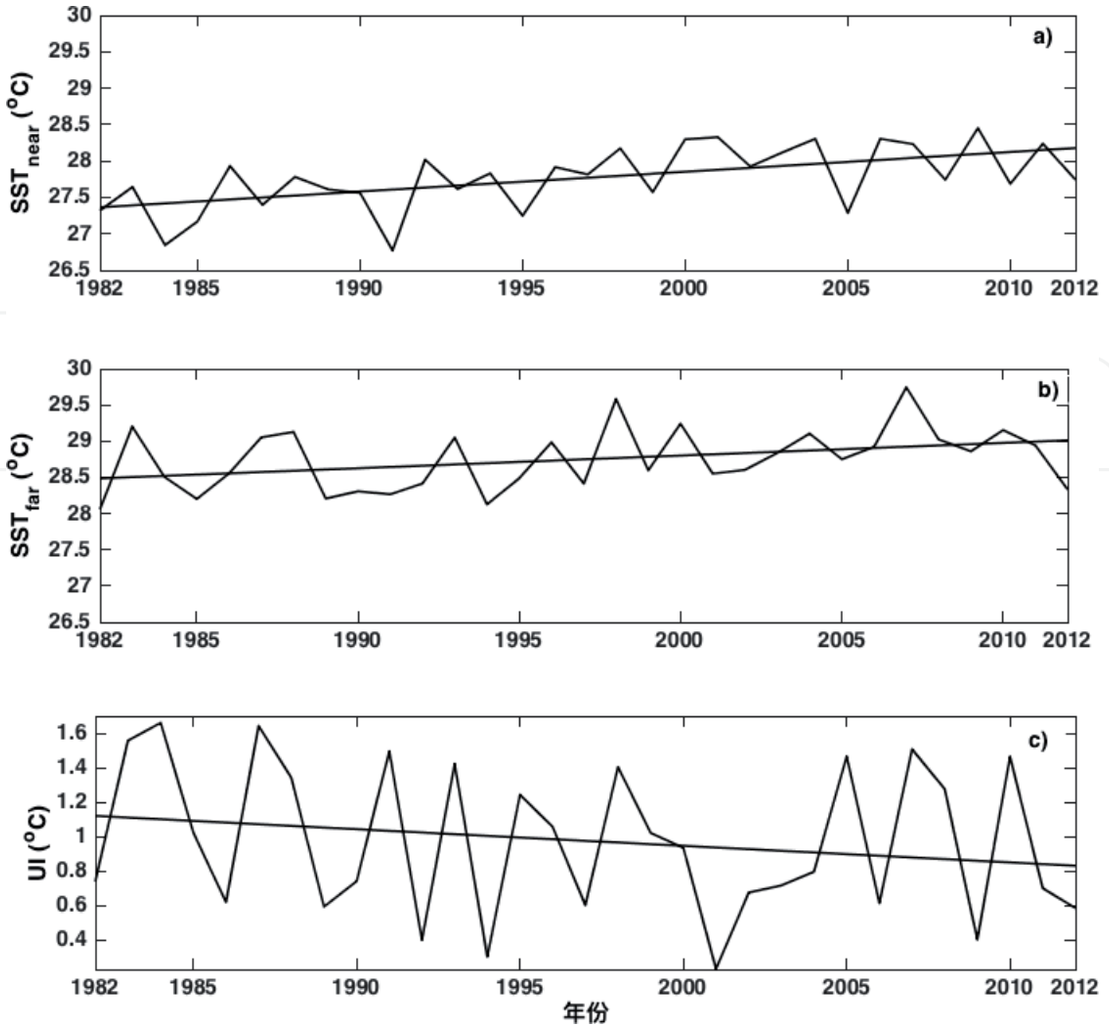

Figure 2.
Variation of the averaged SST in summer in the upwelling zone (zone A in ***Figure 1****) (a) and the background zone in the deep water (zone B in* ***Figure 1****) (b) and the upwelling index (UI) of UEH (c) from 1982 to 2012. The straight lines represent the linear trends of the variations (cited from [26]).*

index (UI) to denote the upwelling intensity (refer to [26] for details). **Figure 2** shows the variation of SST in zones A and B and the UI of the UEH from 1982 to 2012. One can see that both the SST in the upwelling zone A, i.e., SST_{near}, and that in the deep water without upwelling, i.e., SST_{far}, have increasing trends in recent 30 years. The increase rate is 0.03°C/a for zone A and 0.02°C/a for zone B, respectively. The warming in the upwelling zone is faster than that in the open-sea waters. Thus, the UI of the UEH has a decreasing trend with a rate of −0.01°C/a. The UEH weakens as the global climate changes. This is opposite to the intensification in the coastal upwelling zones on the east coast of the ocean basin [22, 24–25, 41].

In order to investigate the interannual variability of the UEH, we decompose the UI time series using the empirical mode decomposition (EMD) method [42]. The first three intrinsic mode functions (IMFs 1–3) are shown in **Figure 3**. One can see that the periods of the IMFs 1–3 are about 3 a, 5 a, and 10 a, respectively. The corresponding variance contributions are 82, 10, and 1%. The IMF1 has the largest amplitude and dominates the interannual variability of the UEH. On the other hand, the 3-year variation is highly related to the ENSO events [33].

2.3 Variability of upwelling center

Taking the latitude of the maximum UI as the upwelling center, one can investigate the variation of the position of the UEH. As shown in **Figure 4a**, one can see

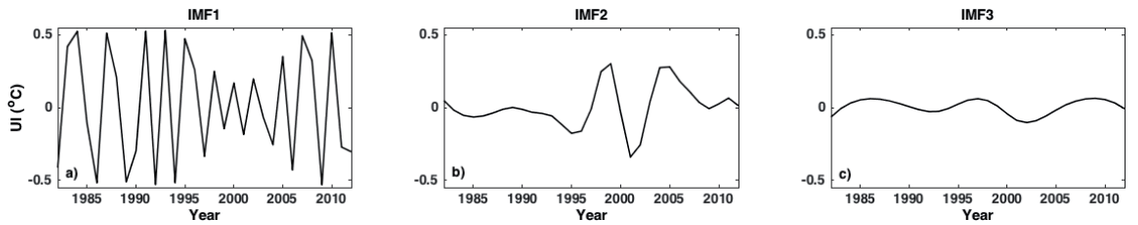

Figure 3.
First three intrinsic mode functions (IMFs 1–3) of the UI series of the UEH (a) IMF1, the first and largest mode, (b) IMF2, the second mode and (c) IMF3, the third mode (cited from [26]).

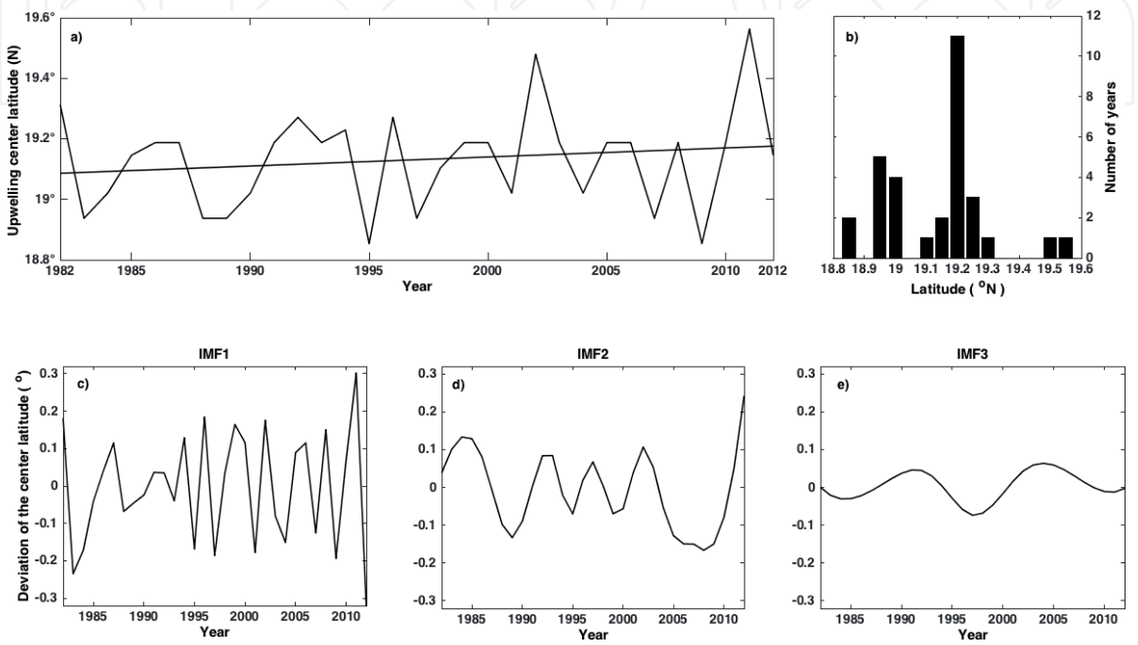

Figure 4.
The interannual variation (a) and the statistics (b) of the upwelling center of the UEH in 1982–2012 and three IMFs of the variation (c–e) (cited from [26]).

that the center of UEH oscillated north-southward along the Hainan coast between 18.9° and 19.3°N in the past 30 years. The center positions of the largest probability are in 19.2°–19.3°N and 18.9°–19°N. For the long-term variation trend, one can see that the center position shifted northward from 1980 to 2012. The IMFs of the center position series also show interannual variability with three intrinsic periods of 3 a, 5 a, and 10 a, of which IMF 1 has the largest amplitude and dominates the variance.

2.4 Effects of wind stress and wind stress curl

The UEH is generally driven by the alongshore wind stress. However, for the long-term variation, the alongshore wind stress has an increasing trend with a rate of 1.1×10^{-5} N/m^2/a as shown in **Figure 5a**. This is opposite to the decreasing trend of the UEH shown in **Figure 2c**. The correlation coefficient of the interannual variability of the UI with that of the alongshore wind stress is only 0.43 ($P < 0.02$). The alongshore wind stress seems not to be the dominant factor for the long-term variation of the UEH. **Figure 5b** shows the variation of the wind stress curl over the upwelling zone. One can see that the wind stress curl has a decreasing trend with a rate of -2.7×10^{-11} N/m^3/a. The correlation coefficient of the wind stress curl and the UI reaches 0.66 ($P < 0.001$). For the first two IFMs, the correlation coefficients reach 0.75 for IMF1 and 0.54 for IMF2 for the wind stress curl but are 0.52 for IMF1 and 0.46 for IMF2 for the alongshore wind stress. This result suggests that the wind

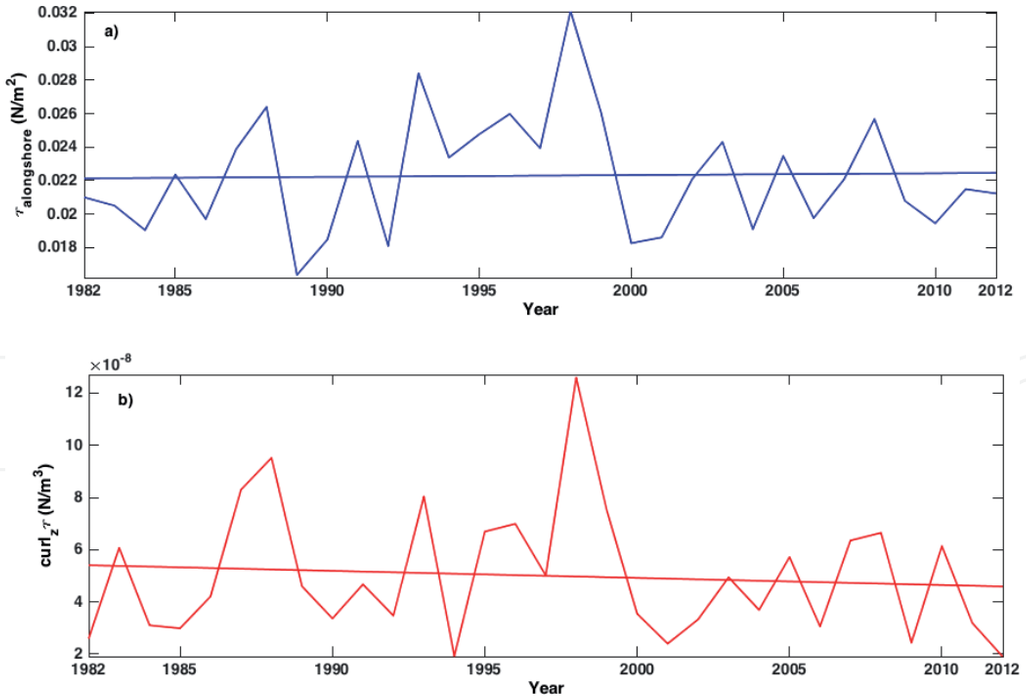

Figure 5.
Variations of the alongshore wind stress $\tau_{alongshore}$ (a) and the curl of wind stress curl$_z\tau$ (b) over the UEH zone in 1982–2012. The straight lines represent the linear trends (cited from [26]).

stress curl-induced Ekman pumping plays a more important role in the long-term variability of the UEH intensity.

By comparing the latitudes of maximum alongshore wind stress (around 19.1°N) and wind stress curl (around 19.25°N), one can see that the latitude of the maximum wind stress curl is more consistent with latitudes of the maximum UI at 19.2°–19.3°N. This shows the importance of the wind stress curl on the long-term variation of the UEH.

3. Response of UEH to super El Niño events

3.1 Background

As mentioned above and in previous studies, the UEH has interannual variability associated with the ENSO events [37]. Comparing with the UEH, the upwelling east of Vietnam coast (UEV) in the western SCS has different response to the ENSO events [8, 43]. Jing et al. [33] analyzed the response of UEH and UEV to a super El Niño event of 1997–1998 and found that in summer 1998, southerly winds were intensified in the northern SCS, so that UEH was strengthened, while easterly winds were abnormally intensified along the Vietnam coast over the southern SCS, so that UEV is weakened. Most of these previous investigations explained the mechanisms of response of coastal upwelling to El Niño events based on wind forcing, and less attentions are paid to the background ocean dynamic processes.

Recently, another super El Niño event occurred in 2015–2016, which lasted for longer than 12 months with sea surface temperature anomaly (SSTA) peaks higher than 2°C for longer than a half year as shown in **Figure 6**. Shen et al. [39] use SST, sea surface height (SSH), wind fields, and heat flux data from 1995 to 2016 to compare different responses of UEH and UEV to the two super El Niño events of 1997–1998 and 2015–2016 and found that ocean mesoscale eddies significantly affected the response of coastal upwelling to El Niño events.

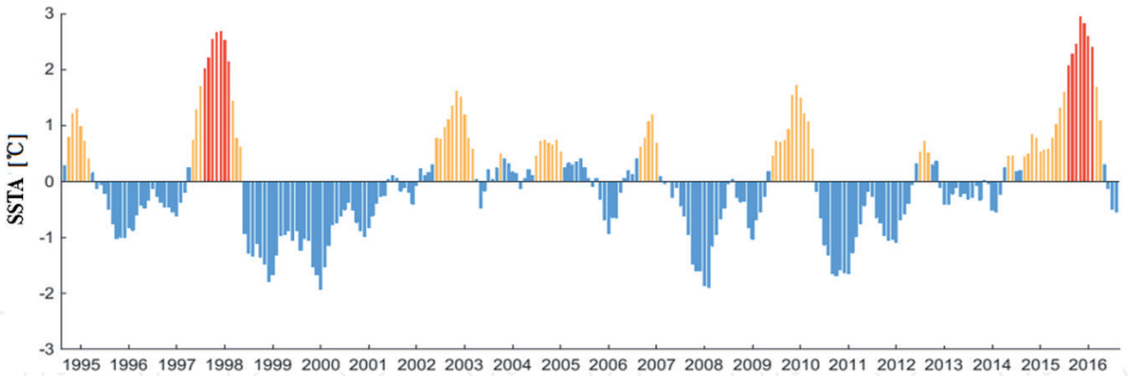

Figure 6.
Niño 3.4 index from 1995 to 2016. Blue, orange, and red color bars represent SSTA lower than 0.4°C, but higher than 0.4 and 2°C, respectively (cited from [39]).

3.2 SSTA

The SSTA with respect to climatologic SST is generally used as an indicator to represent response of upwelling to the El Niño events [8, 33, 43, 44].

Figure 7a–b shows the averaged SSTA fields of UEH and UEV in local summer (June–July–August) of 1998. One can see that the extent of cold water in UEH expanded with totally averaged SST 0.04°C lower than that of climatology, implying that UEH was slightly intensified. On the other hand, the extent of cold water in UEV was remarkably shrunk with greatly increased SSTA. The totally averaged SSTA was 1.15°C. In particular, at the cold center of climatology near 11° 30'N, SSTA was warmed up as high as 1.8°C. This implies that the UEV greatly weakened after the super El Niño event of 1997–1998 ended in spring 1998.

Super El Niño event of 2015–2016 ended in spring 2016 has the longest lifetime and the highest SST anomaly in the equatorial Pacific since 1900. In summer 2016, SSTAs in UEH and UEV are entirely different. As shown in **Figure 7c–d**, all SSTs in UEH show warm anomaly with the SSTA amplitudes of 0.4–1.0°C, and the warmest anomaly appeared at about 100 km offshore. Comparing SST distribution (not shown), the cold water area of UEH greatly decreased, with totally averaged SSTA of 0.67°C, implying that UEH weakened. Meanwhile, SST in the UEV decreased about 0.2°C in the area 50 km offshore from 11° 30'N to 12° 30'N, while SST slowly increased from the cold center to the deep water. The totally averaged SSTA was 0.17°C with a maximum warm anomaly of 0.4°C, implying that UEV was also slightly weakened.

3.3 Wind field anomaly

The variability of local wind field is an important factor that must be considered in response of coastal upwelling to super El Niño events. **Figure 8** shows the wind vector anomaly (arrows) and the wind stress curl anomaly (color) of the UEH and the UEV in summer 1998 and 2016. Forced by abnormal southerly winds and positive wind stress curl anomaly, both favorable conditions for upwelling, UEH was intensified with expanded sea surface cold water area and lower temperature in summer 1998 (**Figure 8a**). This is consistent with SSTA patterns shown in **Figure 7a**. Meanwhile, for the UEV, southerly wind anomaly was remarkable, and wind stress curl decreased with the negative anomaly of -2×10^{-7} N m^{-3}. The two factors restrained the upwelling development, so that SST in UEV increased in summer 1998 (**Figure 8b**). This is consistent with SSTA patterns shown in **Figure 7b**.

In summer 2016, southerly wind anomaly was still dominant over the UEH; the wind stress curl anomaly was positive and negative over the northern and southern

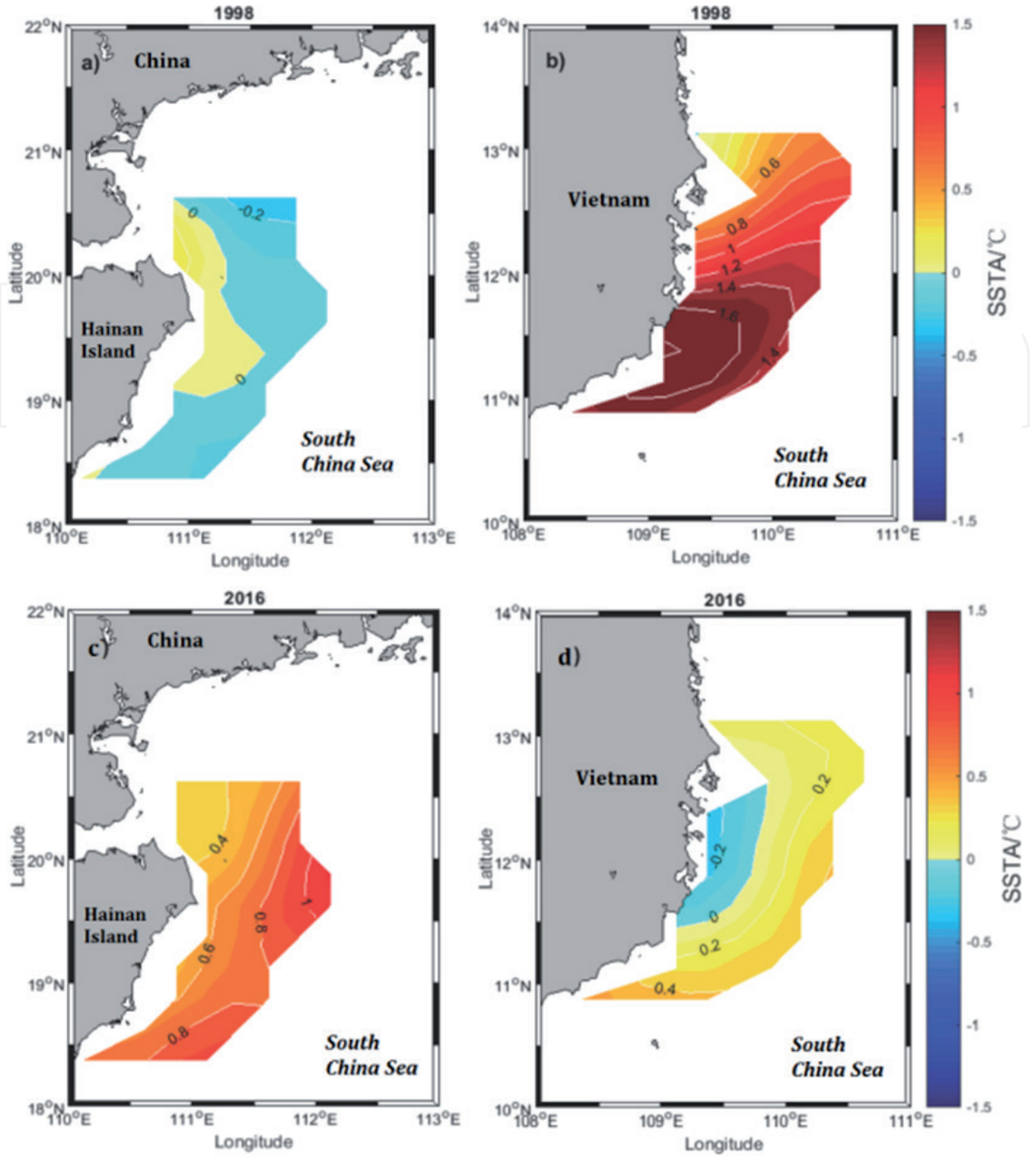

Figure 7.
SSTA in UEH (a, c) and UEV (b, d) in summers 1998 and 2016. Color codes are in °C (cited from [39]).

UEH, respectively (**Figure 8c**). The wind speeds were higher than the climatologic means. Theoretically, the wind fields were favorable to the upwelling development. However, the comparison with the SSTA patterns shown in **Figure 7c** indicates that the temperature in the UEH cold water area greatly increased and the region of cold water became narrower. Based on this fact, Shen et al. [39] speculate that there are other factors to weaken the UEH. In the UEV, the southerly wind anomaly was dominant, and the wind stress curl anomaly was positive in most cases with the mean positive anomaly as high as 1.5×10^{-7} N m^{-3} (**Figure 8d**). The wind speeds were greater than the climatologic values. Such wind field anomaly was greatly favorable to the upwelling development. However, results in the above section indicate that in summer 2016, the mean SST in the UEV was close to the climatologic mean, cold water area was not obviously expanded, and lower SST appeared in partial area only. This implies that there are some factors to counteract forcing of wind field, resulting in unchanged upwelling intensity in the UEV.

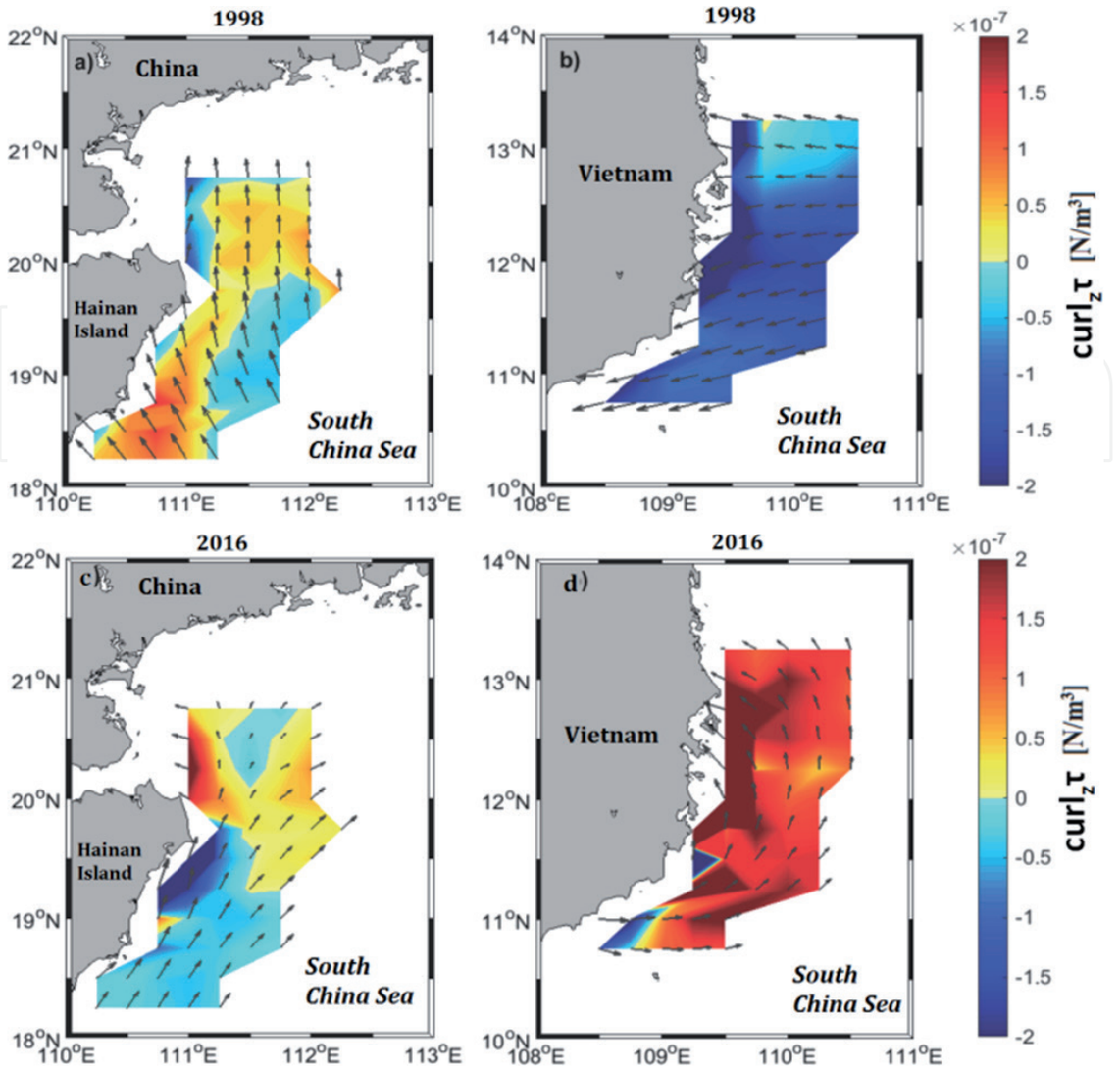

Figure 8.
Composite maps of wind vector anomaly (arrows) and wind stress curl anomaly (color codes in N m^{-3}) of UEH (a, c) and UEV (b, d) in summer 1998 and 2016 (cited from [39]).

3.4 Surface heat flux

The sea surface heat flux is an important factor to affect the SSTA. **Figure 9a** shows summer mean net heat flux of the western SCS in 1998 and 2016. One can see that the horizontal distributions are characterized by dipole patterns, i.e., a low-value center, located at the deep basin coexisting with a high-value center at the northwestern shelf. The extent of high net heat flux (NHF) (>7.5 × 10^6 J m^{-2}) in summer 2016 (**Figure 9b**) was much larger than that in summer 1998 (**Figure 9a**), suggesting that the heat absorbed by UEH and UEV was higher than that in 1998 summer.

Figure 9c shows the difference of spatial mean NHF in summer 2016 from that in summer 1998. For both of the UEH and the UEV, all the heat flux differences are positive, i.e., the heat gain due to shortwave solar radiation in summer 2016 was greater than that in summer 1998, and the heat losses due to the long-wave radiation, latent heat flux, and sensible heat flux were smaller than that in summer 1998. This result reveals that NHF absorbed by the sea water of two upwelling zones in summer 2016 was near twice of that in summer 1998. The increase amplitude of the NHF in UEV was twice of that in UEH. However, comparing that in summer 1998, the mean SST in UEH in summer 2016 increased near 0.71°C, while that in UEV decreased by 0.98°C as shown in **Figure 7**, namely, in the UEV, the NHF increased, but SST decreased. Therefore, the NHF is not a dominant factor to

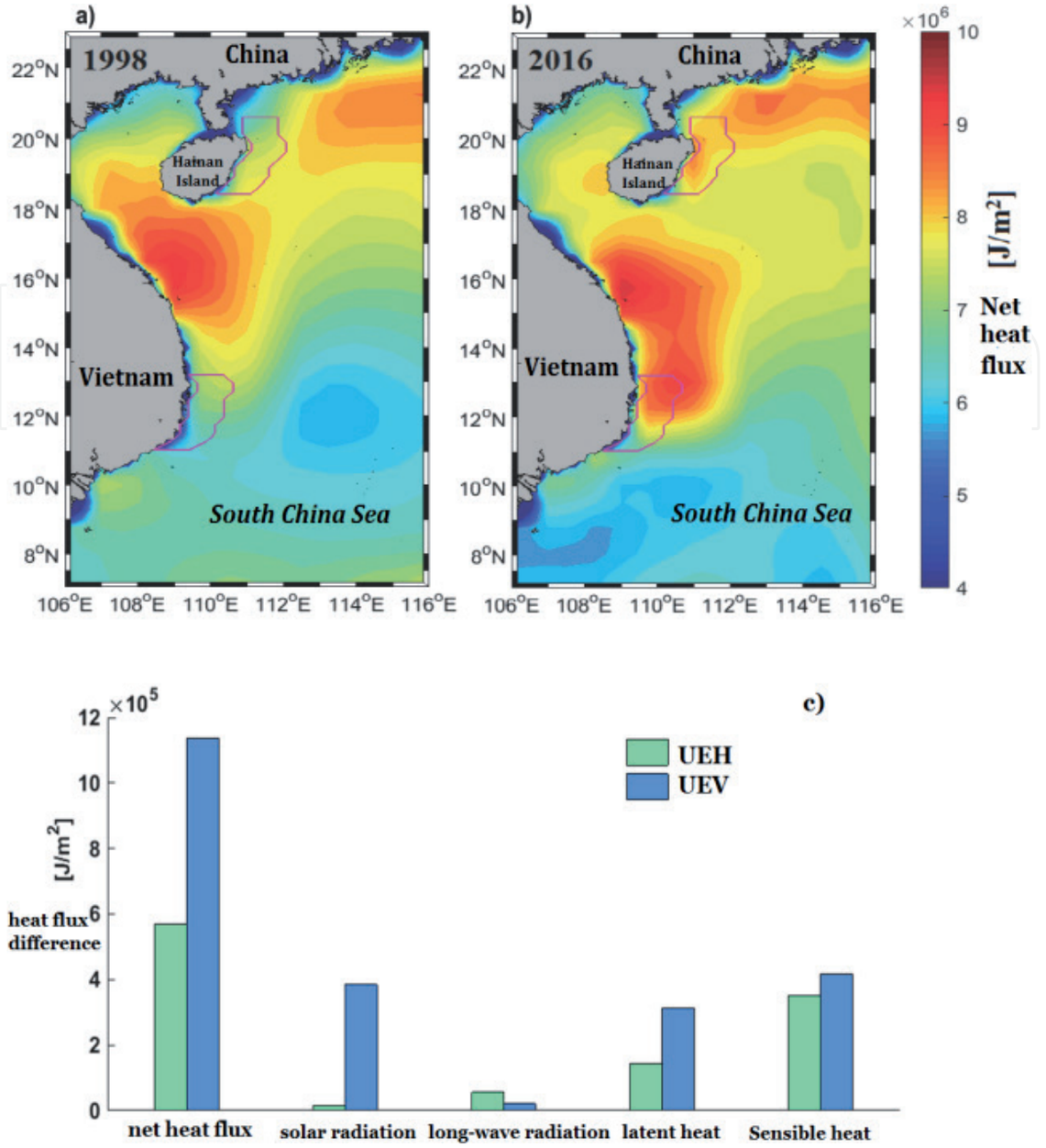

Figure 9.
Downward mean net heat flux (NHF) in the western SCS in summer 1998 (a) and 2016 (b) and difference of mean heat fluxes of summer 2016 from 1998 in UEH and UEV (c). Color codes in a–b represent NHF in J m^{-2} (cited from [39]).

affect SSTA in the upwelling cold water area during the El Niño events, but there must be other dynamic factors to counteract the SST increase in the upwelling cold water areas.

3.5 Effects of ocean dynamic processes on upwelling cold water

As a component of the ocean circulation, coastal upwelling is affected by the background current. The surface cold water in the upwelling zone is formed by transport of cold water in lower layers to upper layers carried by the vertical motion of sea water. Meanwhile, if horizontal currents transport water masses with different properties from other areas to the upwelling zone, or alter the current fields to affect divergence of upper layer sea water, it is possible to change the intensity and location of upwelling.

Mesoscale eddies are active in the SCS [45, 46]. The horizontal and vertical motions of eddies would modulate background current and mass transport, so

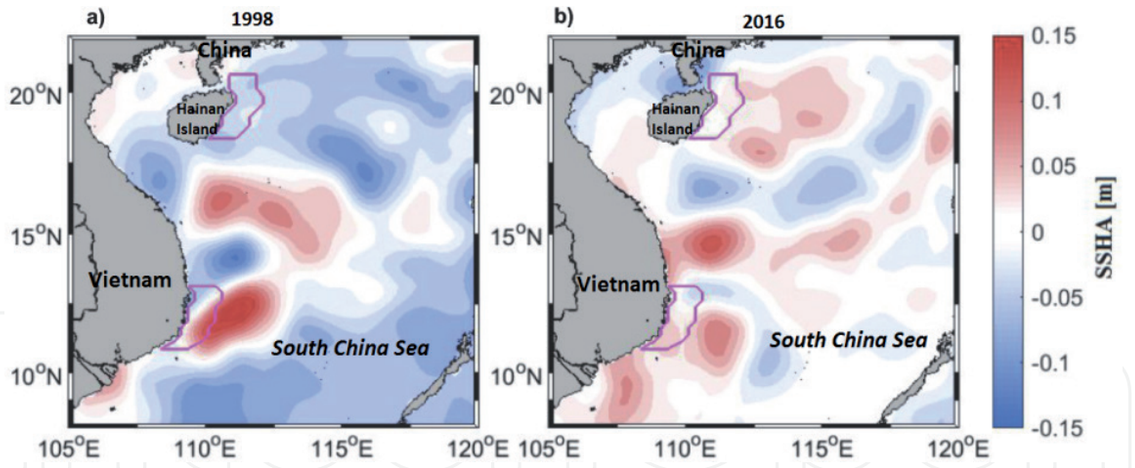

Figure 10.
SSHA distribution in the western SCS in summer 1998 (a) and 2016 (b). Color codes are in m (cited from [39]).

that they may be the important processes to affect UEH and UEV. Here, the SSH anomaly (SSHA) is used as an index to analyze effects of mesoscale eddies on SSTA in the upwelling zones. **Figure 10** shows SSHA distribution in the western SCS in summer 1998 and 2016. In summer 1998, SSHA in the northern SCS was negative (**Figure 10a**), favorable for UEH development. Meanwhile, there was an ellipse-shaped warm eddy in SW-NE direction off the South Vietnam coast. The UEV was located within the extent of warm eddy, so that the UEV was restrained. On the other hand, in summer 2016, the UEH was located in the positive SSHA area, and there were multiple weak warm eddies east of Hainan Island (**Figure 10b**). The SSHA was also positive in the offshore water of Vietnam. Near the Indo-China Peninsula, there were a train of stronger warm eddies centered at 10°, 12°, and 15°N, respectively. This might explain that although the wind field anomaly along the Vietnam coast was quite favorable for upwelling development, the extent of cold water did not expand, and SST also did not decrease with respect to the climatology. It is the warm eddies that may counteract the wind forcing effect.

4. Response of UEH to typhoon passage

4.1 Statistics of typhoon

Previous investigators have addressed that the hydrological characteristics and dynamic structure of the upwelling may have dramatic changes after typhoon passage [28, 38, 47]. The UEH is located in the pathway of typhoons formed both in the western Pacific Ocean and the SCS [47, 48]. In order to investigate the sudden impact of typhoon forcing on the UEH, Xie et al. [31] analyzed the statistics of typhoons passing the UEH zone during the past 34 years from 1982 to 2015.

As shown in **Figure 11**, there were a total of 42 tropical cyclones passing the UEH between April and September from 1982 to 2015, of which 24 cyclones originated from the western Pacific and 18 from the SCS. The cyclones originating from the Pacific passed over the UEH mostly in July, while the locally generated cyclones in the SCS appeared mostly in August. Most cyclones moved northwestward into the research area, while several cases passed this region north-/northwestward or even parallel to the coastline. **Figure 11g** shows the incidence angles of the cyclones, which is defined as the angle between the pathway of cyclone when entering the upwelling region and the trend of coastline, i.e., 0° for the passage parallel to the coastline and 90° for perpendicular. Twenty-five cyclones entered this area with

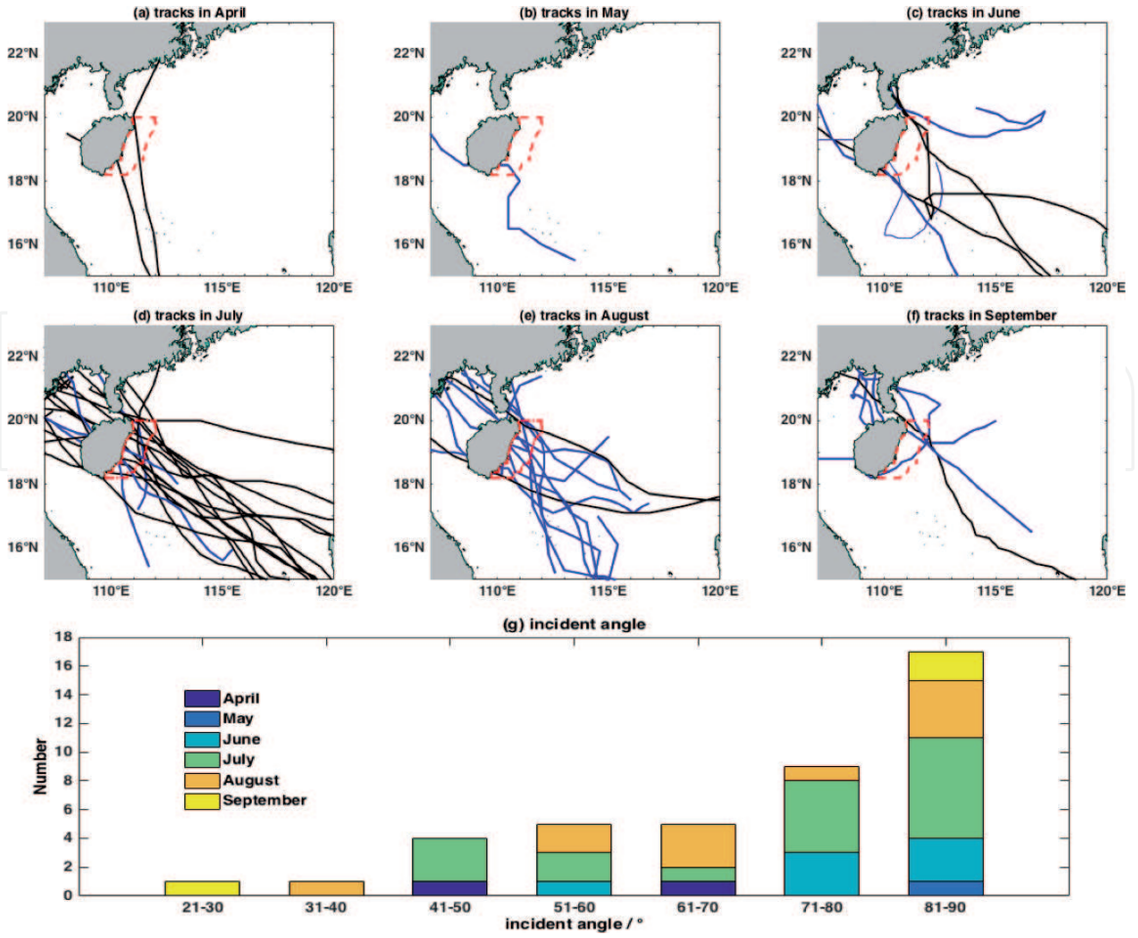

Figure 11.
Tracks and incidence angles of cyclones passing over the UEH zone (red box) during the period from April to September of 1982 to 2015. Black lines in (a)–(f) are tracks of tropical cyclones originated from the Pacific and blue lines from the SCS. Red boxes represent the UEH zone for statistics (cited from [31]).

incidence angle between 70° and 90°, among which seventeen passages were nearly perpendicular to the coastline (80°–90° of the incidence angle). Only in two cases the incidence angles were smaller than 40°.

As for the monthly distribution, the passages of tropical cyclones were prevailing in summer from June to August, when upwelling had been well developed. There are 36 cases in summer, accounting for 86% of all passing cyclones, in which 18 cases occurred in July. As of the cyclone intensity, the most frequent category was severe tropical storm (STS) with 12 cases during 34 years, followed by the tropical depression (TD) and typhoon (TY) of 10 and 9 cases, respectively. The three most prevailing types account for 74% of all passing tropical cyclones. The severest super typhoon (super TY) occurred in July 2014.

4.2 Statistics of SST variation

The SST variations in the UEH induced by cyclone passages during 1982 and 2015 are shown in **Figure 12**. The SST difference (ΔSST) between the post-cyclone and pre-cyclone values is used to specify the response of UEH to typhoon passages. Here the pre- and post-SST are averaged values of the whole region within 7 days before cyclones enter or after passing the upwelling zone (outlined by red dashed lines in **Figure 11**), respectively. In most cases, the SST in the upwelling zone decreased ($\Delta SST < 0$) after the typhoon passage, with the greatest decrease of −2.4°C induced by the severe typhoon (STY) Zeke in 1991. The SST increase occurred in 1985, 1989, and 2001, with the greatest increase of 3.4°C after the passage of a nameless weak

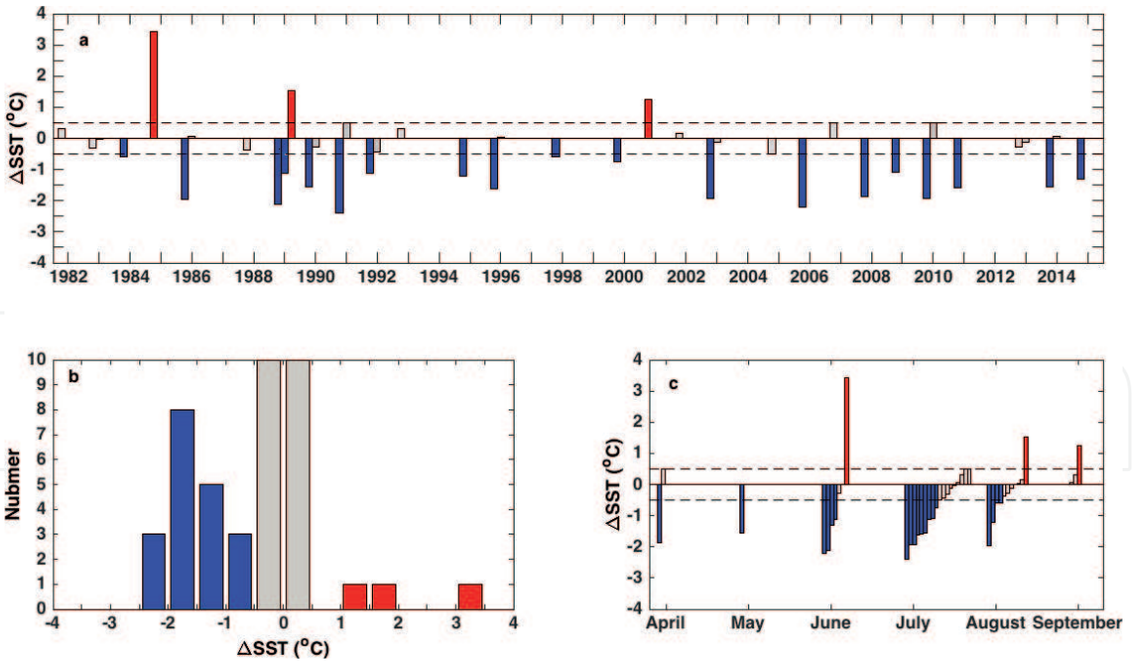

Figure 12.
SST changes induced by the 42 tropical cyclones passing over the UEH from 1982 to 2015. (a) Yearly distribution. (b) Number of typhoons in different cases. (c) Monthly distribution. Warming cases are in red, cooling cases in blue, and no-significant-change cases in gray (cited from [31]).

tropical depression (WTD). The warming of sea surface after typhoon passages is distinguished from the prevailing cooling in the open ocean.

All 42 cases are categorized into three types according to the SST variation ΔSST: cooling with $\Delta SST < -0.5$°C, no-significant-change with $-0.5 \leq \Delta SST \leq 0.5$°C, and warming with $\Delta SST > 0.5$°C. The statistical result is listed in **Figure 12b**. Nineteen cases of forty-two cyclones triggered surface cooling, with ΔSST concentrated mainly between −2 and −1.5°C and averaged to −1.5°C; twenty cases were in the category of no-significant-change with a mean value of 0°C, accounting for 48% of all cases and the number of slightly warming is larger than that of slightly cooling; three warming cases were found with a mean value of 2.1°C. The magnitude of averaged warming is greater than that of cooling.

In monthly distribution (**Figure 12c**), most warming cases occurred from June to September, with a maximum in June. The largest magnitude and most frequent cooling were in July, preceding that in June and August.

4.3 SST changes vs. typhoon parameters

It is usually assumed that the intensity and moving speed of tropical cyclone are two predominant factors influencing SST decrease in the open ocean. The stronger or slower-moving cyclones are supposed to induce more SST decrease [49]. Other studies suggested that the incidence angle and path of tropical cyclone may also play an important role in SST variation in coastal regions [29, 50]. In the UEH, all the four mentioned parameters are analyzed in 42 cases from 1981 to 2015.

The distributions of ΔSST on two joint parameters are illustrated in **Figure 13**. One can see that all three warming cases occurred after passage of low-wind-speed tropical cyclones, with duration period of 5–9 h, and the magnitude of SST variation increases with the incidence angle. For cooling cases, the relation between SST variation and maximal wind speed is not significant, with correlation coefficient $R^2 = 0.29$. The magnitude of SST decrease is not dependent on the duration period of tropical cyclone. Most cooling cases occurred after tropical cyclones with the

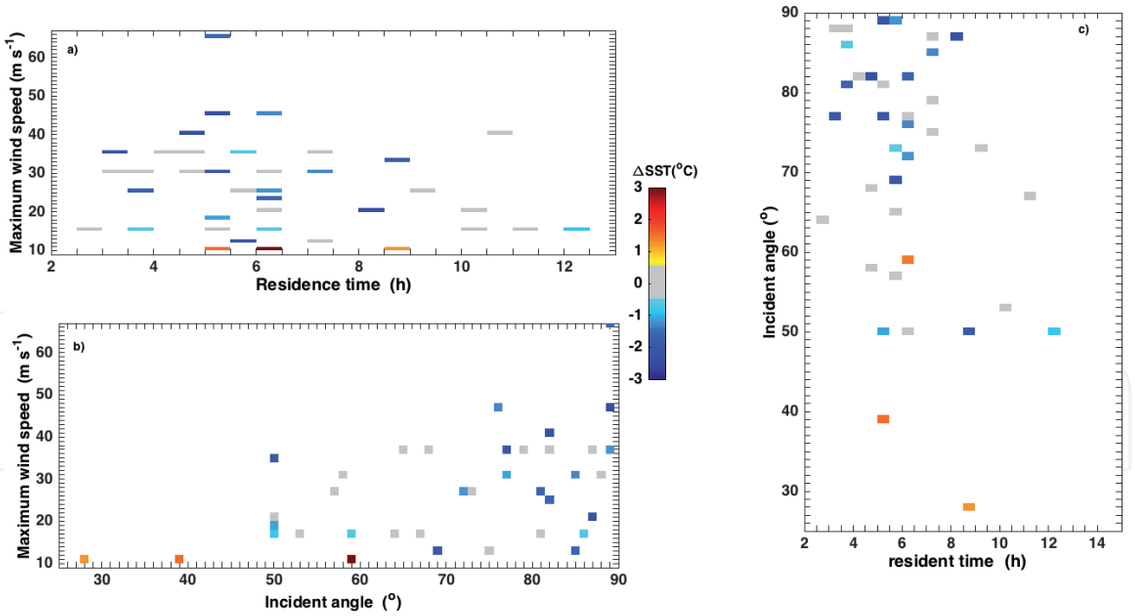

Figure 13.
2-D distribution of SST variation with tropical cyclone parameters (a) SST variation vs. maximum wind speed and residence time. (b) SST variation vs. maximum wind speed and incident angle. (c) SST variation vs. incident angle and residence time (cited from [31]).

duration time smaller than 8 h. All cooling cases occurred with the incidence angles greater than 50°, and there is an increasing trend of ΔSST magnitude with the incidence angle. The SST variation in no-significant-change is independent of the wind speed or the duration time of tropical cyclone. The incidence angles were all larger than 50°. It seems that the maximal wind speed and the incidence angle contribute more to the SST response, and the duration time might have slight influence.

4.4 Mechanisms of SST change

The change in SST induced by passage of tropical cyclone depends on the net heat flux in the research area. As a severe local disturbance, strong vertical convection and turbulent mixing during the momentum transfer from the cyclone to the sea water are generally regarded as the primary mechanism for sea surface cooling [47]. The magnitude of cooling increases as the strength of the cyclone increases or the movement speed decreases, due to the enhancement of vertical pumping and mixing. Generally, the heat variations of the upper ocean due to vertical convection and mixing induced by tropical cyclone, denoted as Q_v and Q_m, respectively, are negative. However, 20 no-significant-changes and even 3 warming cases appear in the above statistical analysis, indicating that there are other mechanisms inducing the positive heat flux via tropical cyclones.

As illustrated in **Figure 14**, the typhoon approaching the upwelling zone might decrease or increase the SST in the offshore water due to onshore or offshore Ekman transport induced by the typhoon winds. The heat flux due to the typhoon Ekman flow is denoted by Q_E, and its sign depends on the relative locations of the typhoon track and the upwelling zone [29]. For three SST warming cases mentioned above, the locations of tropical cyclone tracks relative to the upwelling zone are variant: one was south to the upwelling core, one passed the central upwelling zone, and one veered from the north to the south. The local typhoon-induced heat advection Q_{Ea} by Ekman transport is merely one factor influencing the SST variation.

Zheng et al. [50] suggested that typhoon could force a single sea-level soliton in the deep offshore water with the positive amplitude. Warm water was thus transported onshore with the shoreward propagation of the soliton due to nonlinearity and resulted in net positive heat flux shoreward. The onshore amplitude of

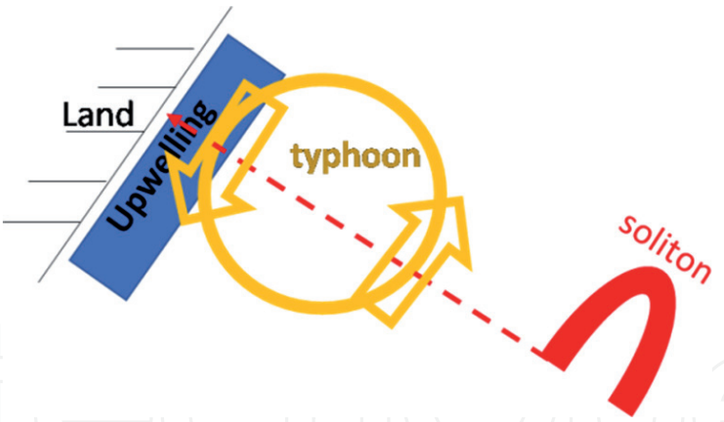

Figure 14.
Sketch of typhoon-induced upwelling-favorable/upwelling-unfavorable wind and shoreward propagating soliton.

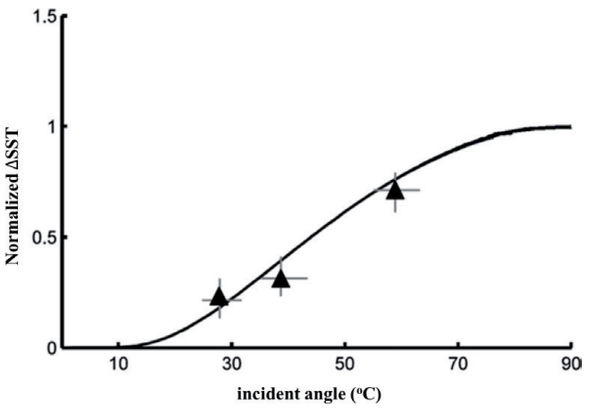

Figure 15.
SST variation vs. incidence angle of tropical cyclone for three SST warming cases in UEH (cited from [31]).

soliton induced by typhoon (thus the heat advection marked as Q_{ra}) depends on the typhoon incidence angle, i.e.,

$$\beta_d \cong \alpha_1 sin^{1/2}\theta \, exp\left(-\frac{\alpha_2}{sin\theta}\right) \tag{1}$$

in which β_d is the amplitude of soliton, θ the typhoon incidence angle, and α_1 and α_2 are parameters related to the continental shelf width, the turbulent viscosity and the propagation velocity of the soliton (refer to [50] for detail).

The normalized SST variation vs. the incidence angle of tropical cyclone in three warming cases is shown in **Figure 15**. One can see that the normalized ΔSST increases with the incidence angle and conforms to the idealized curve suggested by Zheng et al. [50]. It shows that the heat transport by the offshore soliton is a significant mechanism of SST increase in UEH after typhoon passages.

To sum up, the heat flux induced by tropical cyclone in UEH consists of two main categories: nonlocal heat transport Q_r through shoreward transport of the offshore warm water by the tropical cyclone induced soliton, here $Q_r = Q_{ra}$ and is positive; local heat flux by the momentum input of tropical cyclone Q_1, including the heat change due to vertical convection/mixing Q_{vm} (negative) and Ekman flow Q_{Ea} (positive/negative), here $Q_1 = Q_{vm} + Q_{Ea}$. Thus, the net heat flux by tropical cyclone is summarized as

$$Q_{net} = Q_r + Q_1 \begin{cases} > 0 & if\ Q_1 > 0\ or\ Q_r > \\ = 0 & if\ Q_1 < 0\ and\ Q_r = -Q_1 \\ < 0 & if\ Q_1 < and\ Q_r < -Q_1 \end{cases} \tag{2}$$

The above statistics of 42 tropical cyclone passages indicate that the SST response in the UEH could be warming, no-significant-change, or cooling, accounting for 7, 48, and 45%, respectively. The heat flux is affected by the intensity, the moving speed, the incidence angle, and the relative location of tropical cyclone. The combination of these factors modifies the relative magnitudes of Q_r and Q_1, thus influences the SST response signatures.

5. Summaries

The wind-driven UEH is a typical seasonal coastal upwelling in the northwestern SCS. Satellite SST data and wind products help to investigate the variability of UEH to multi-scale atmospheric processes. This chapter overviews the recent progress, including the long-term and interannual variability of UEH with the global climate change in recent decades, the response of UEH and UEV to super El Niño events in 1998 and 2016, the variation of UEH after sudden impacts of typhoon passages, and the variability mechanisms. The main results are summarized as follows:

1. Different from intensification trend of most east-coast upwelling, the UEH has a weakened trend in the recent 30 years from 1982 to 2012. The decreasing rate of UI is 0.01°C/a. The UEH has higher correlation coefficient with the variation of the local wind curl, which also has decreasing trend than the alongshore wind stress. Meanwhile, the latitude of UEH core tends to move northward, so does the latitude of the maximum wind curl location. Three intrinsic modes with periods of 3, 5, and 10 years are found both for the upwelling intensity and the core location variation, of which the mode with a 3-year period dominates the variation. The local wind curl plays an important role in the interannual variation of the UEH.

2. The response of the UEH to the super El Niño event in 2016 was different from that in 1998. The responses of the UEH to two super El Niño events were also different from that of the UEV. Specifically, the upwelling-favorable wind anomaly enhanced the UEH, while the upwelling-unfavorable wind anomaly weakened the UEV in summer 1998. In summer 2016, there were upwelling-favorable wind anomalies in both the UEH and the UEV. However, the cool water zone shrunk with warmer SSTA in the UEH region, and the UEV became warmer, indicating other mechanisms beside the ENSO-induced wind anomaly. It is found that mesoscale eddies may significantly affect the response of upwelling to super El Nino events.

3. There are three categories of SST response for 42 cases of typhoons passing through the UEH from 1982 to 2015, i.e., increasing SST (19 cases), no-significant-changing SST (20 cases), and decreasing SST (3 cases). The averaged SST increase is 2.1°C, higher than the averaged decrease of −1.5°C. The intensity and the incidence angle are found to be main factors affecting the variation of SST. The typhoon-induced elevation nonlinear soliton transports heat from the open ocean to the coastal upwelling zone, so that SST increases. The observed SST variation vs. the incidence angle of typhoon track conforms to the theoretical predictions, namely, the SST variation may be caused by both local and remote heat transports induced by typhoon.

Acknowledgements

This work is supported by the National Natural Science Foundation of China [Grant Numbers 41776034, 41476009, and 41676008]; the National Program on Global Change and Air-Sea Interaction [Grant Numbers GASI-02-SCS-YGST2-02 and GASI-IPOVAI-01-02]; the Project of Enhancing School with Innovation of Guangdong Ocean University [Grant Number CYL2019231419012].

Author details

Lingling Xie* and Mingming Li
College of Ocean and Meteorology, Guangdong Ocean University, Zhanjiang, China

*Address all correspondence to: llingxie@163.com

References

[1] Huyer A. Coastal upwelling in the California current system. Progress in Oceanography. 1983;**12**(3):259-284. DOI: 10.1016/0079-6611(83)90010-1

[2] Smith RL. Coastal upwelling in the modern ocean. Geological Society London Special Publications. 1992;**64**(1):9-28

[3] Cropper TE, Hanna E, Bigg GR. Spatial and temporal seasonal trends in coastal upwelling off Northwest Africa, 1981-2012. Deep Sea Research Part I. 2014;**86**:94-111. DOI: 10.1016/j.dsr.2014.01.007

[4] Silva A, Palma S, Oliveira PB, Motia MT. Composition and interannual variability of phytoplankton in a coastal upwelling region (Lisbon Bay, Portugal). Journal of Sea Research. 2009;**62**(4):238-249. DOI: 10.1016/j.seares.2009.05.001

[5] Kuvaldina N, Lips I, Lips U, Liblik T. The influence of a coastal upwelling event on chlorophyll A and nutrient dynamics in the surface layer of the Gulf of Finland, Baltic Sea. Hydrobiologia. 2010;**639**(1):221-230. DOI: 10.1007/s10750-009-0022-4

[6] Suess E, Thiede J. Coastal Upwelling its Sediment Record: Part A: Responses of the Sedimentary Regime to Present Coastal Upwelling. Berlin: Springer Science & Business Media; 2013. DOI: 10.1007/978-1-4615-6651-9

[7] Hu DX. Upwelling and sedimentation dynamics. I. The role of upwelling in sedimentation in the Huanghai Sea and East China Sea—A description of general features. Chinese Journal of Oceanology & Limnology. 1984;**2**(1):13-19. DOI: 10.1007/BF02888388

[8] Xie SP, Xie Q, Wang DX, Liu WT. Summer upwelling in the South China Sea and its role in regional climate variations. Journal of Geophysical Research. 2003;**108**(C8):3261. DOI: 10.1029/2003JC001867

[9] Zheng Z-W, Zheng QA, Kuo Y-C, Gopalakrishnan G, Lee C-Y, Ho C-R, et al. Impacts of coastal upwelling off East Vietnam on the regional winds system: An air-sea-land interaction. Dynamics of Atmospheres & Oceans. 2016;**76**(1):105-115. DOI: 10.1016/j.dynatmoce.2016.10.002

[10] Ianson D, Feely RA, Sabine CL, Juranek LW. Features of coastal upwelling regions that determine net air-sea CO_2 flux. Journal of Oceanography. 2009;**65**(5):677-687. DOI: 10.1016/j.dsr.2014.01.007

[11] Lachkar Z, Gruber N. Response of biological production and air-sea CO_2 fluxes to upwelling intensification in the California and canary current systems. Journal of Marine Systems. 2013;**109-110**:149-160. DOI: 10.1016/j.jmarsys.2012.04.003

[12] Li L. Summer upwelling system over the northern continental shelf of the South China Sea a physical descriptor. In: Su J, Chuang WS, Hsurh RY, editors. Proceedings of the Symposium on the Physical and Chemical Oceanography of the China Seas. Beijing: China Ocean Press; 1993. pp. 58-68

[13] Gan JP, Allen JS. Modeling upwelling circulation off the Oregon coast. Journal of Geophysical Research. 2005;**110**:C10S07. DOI: 10.1029/2004JC002692

[14] Schafstall J, Dengler M, Brandt P, Bange H. Tidal-induced mixing and diapycnal nutrient fluxes in the Mauritanian upwelling region. Journal of Geophysical Research Oceans. 2015;**115**(C10). DOI: 10.1029/2009JC005940

[15] Hu JY, Wang XH. Progress on upwelling studies in the China seas. Reviews of Geophysics. 2016;**54**(3): 657-673. DOI: 10.1002/2015RG000505

[16] Xie LL, Zhang SW, Zhao H. Overview of studies on Qiongdong upwelling. Journal of Tropical Oceanography. 2012;**31**(4):35-41. DOI: 10.3969/j.issn.1009-5470.2012.04.005 (in Chinese)

[17] Chegini F, Lu Y, Katavouta A, Ritchie H. Coastal upwelling off southwest nova scotia simulated with a high resolution baroclinic ocean model. Journal of Geophysical Research. 2018;**123**(4):2318-2331. DOI: 10.1002/2017JC013431

[18] Joseph KA, Jayaram C, Nair A, George MS, Balchand AN, Pettersson LH. Remote sensing of upwelling in the Arabian Sea and adjacent near-coastal regions. In: Barale V, Gade M, editors. Remote Sensing of the Asian Seas. Cham: Springer; 2019. DOI: 10.1007/978-3-319-94067-0_26

[19] Shetye SR, Shenoi SSC, Gouveia AD, Michael GS, Sundar D, Nampoothiri G. Wind-driven coastal upwelling along the western boundary of the bay of Bengal during the southwest monsoon. Continental Shelf Research. 1991;**11**(91):1397-1408. DOI: 10.1016/0278-4343(91)90042-5

[20] Belmadani A, Echevin V, Codron F, Takahashi K, Junquas C. What dynamics drive future wind scenarios for coastal upwelling off Peru and Chile? Climate Dynamics. 2017;**43**(7-8):1-22. DOI: 10.1007/s00382-013-2015-2

[21] Xie LL, Enric P-S, Zheng QA, Zhang SW, Zong XL, Yi XF, et al. Diagnosis of 3D vertical circulation in the upwelling and frontal zones east of Hainan Island. China. Journal of Physical Oceanography. 2017a;**47**(4):755-774. DOI: 10.1175/JPO-D-16-0192

[22] Bakun A. Global climate change and intensification of coastal ocean upwelling. Science. 1990;**247**(4939):198-201. DOI: 10.1126/science.247.4939.198

[23] Vargas G, Pantoja S, Rutllant José A, Lange CB, Ortlieb L. Enhancement of coastal upwelling and interdecadal ENSO-like variability in the Peru-Chile current since late 19th century. Geophysical Research Letters. 2007;**34**(13):L13607. DOI: 10.1029/2006gl028812

[24] Wang DW, Gouhier TC, Menge BA, Ganguly AR. Intensification and spatial homogenization of coastal upwelling under climate change. Nature. 2015;**518**(7539):390-394. DOI: 10.1038/nature14235

[25] Sydeman WJ, Garcíareyes M, Schoeman DS, Rykaczewski RR, Thompson SA, Black BA, et al. Climate change. Climate change and wind intensification in coastal upwelling ecosystems. Science. 2014;**345**(6192): 77-80. DOI: 10.1126/science.1251635

[26] Xie LL, Zong XL, Yi XF, Li M. Interannual variation and long-term trend of Qiongdong upwelling. Oceanologica et Limnologia Sinica. 2016;**47**(1):1-9 (in Chinese)

[27] Xiu P, Chai F, Curchitser EN, Castruccio FS. Future changes in coastal upwelling ecosystems with global warming: The case of the California current system. Scientific Reports. 2866;**8**:2018. DOI: 10.1038/s41598-018-21247-7

[28] Rao AD, Babu SV, Dube SK. Impact of a tropical cyclone on coastal upwelling process. Natural Hazards. 2004;**31**:415-443. DOI: 10.1023/B:NHAZ.0000023360.37260.5b

[29] Pan AJ, Guo XG, Xu JD, Jiang H, Wan XF. Responses of Guangdong coastal upwelling to the summertime typhoons of 2006. Science China Earth

Sciences. 2012;**55**(3):495-506. DOI: 10.1007/s11430-011-4321-z

[30] Xu JD, Cai SZ, Xuan LL, Qui Y, Zhu DY. Study on coastal upwelling in eastern Hainan I land and western Guangdong in summer 2006. Hiayang Xuebao. 2013;**35**(4):11-18. DOI: 10.3969/j.issn.0253-4193.2013.04.002 (in Chinese)

[31] Xie LL, He CF, Li MM, Tian JJ, Jing ZY. Interannual variation and long-term trend of Qiongdong upwelling. Advances in Marine Science. 2017;**35**(1):1-13. DOI: 10.3969/j.issn.1671-6647.2017.01.002 (in Chinese)

[32] Guo F, Shi MC. Two-dimensional diagnosis model to calculate upwelling on offshore of the east coast of Hainan Island (in Chinese). Acta Oceanologica Sinica. 1998;**20**:109-116

[33] Jing ZY, Qi YQ, Du Y. Upwelling in the continental shelf of northern South China Sea associated with 1997-1998 El Niño. Journal of Geophysical Research. 2011;**116**(C2). DOI: 10.1029/2010JC006598

[34] Wang DK, Wang H, Li M, Liu GM, Wu XY. Role of Ekman transport versus Ekman pumping in driving summer upwelling in the South China Sea. Journal of Ocean University of China. 2013;**12**(3):355-365. DOI: 10.1007/s11802-013-1904-7

[35] Su J, Pohlmann T. Wind and topography influence on an upwelling system at the eastern Hainan coast. Journal of Geophysical Research. 2009;**114**(C6). DOI: 10.1029/2008JC005018

[36] Jing ZY, Qi YQ, Du Y, Zhang SW, Xie LL. Summer upwelling and thermal fronts in the northwestern South China Sea: Observational analysis of two mesoscale mapping surveys. Journal of Geophysical Research. 2015;**120**:1993-2006. DOI: 10.1002/2014JC010601

[37] Liu Y, Pend ZC, Wei GJ, Chen T, Sun W, He J, et al. Variations of summer coastal upwelling at northern South China Sea during the last 100 years. Geochimica. 2009;**38**(4):314-319 (in Chinese)

[38] Su J, Xu MQ, Pohlmann T, Xu DF, Wang DR. A western boundary upwelling system response to recent climate variation (1960-2006). Continental Shelf Research. 2013;**57**:3-9. DOI: 10.1016/j.csr.2012.05.010

[39] Shen YF, Jing ZY, Tan KY, Xie LL. Comparison of responses of the Qiongdong upwelling and the Vietnam coastal upwelling to super El Nino events. Advance in Marine Science. 2019;**37**(3):374-386

[40] Li MM, Xie LL, Zong XL, Zhang SW, Zhou L, Li JY. The cruise observation of turbulent mixing in the upwelling region east of Hainan Island in the summer of 2012. Acta Oceanologica Sinica. 2018;**37**(9):1-12. DOI: 10.1007/s13131-018-1260-y

[41] Santos F, Gomez-Gesteira M, Decastro M, Alvarez I. Differences in coastal and oceanic SST trends due to the strengthening of coastal upwelling along the Benguela current system. Continental Shelf Research. 2012;**34**: 79-86. DOI: 10.1016/j.csr.2011.12.004

[42] Huang NE, Shen Z, Long SR. The empirical mode decomposition and the Hilbert spectrum for nonlinear and non-stationary time series analysis. Proceedings of the Royal Society of London A: Mathematical, Physical and Engineering Sciences. 1998;**454**(1971):903-995. DOI: 10.1098/rspa.1998.0193

[43] Kuo NJ, Zheng QA, Ho CR. Response of Vietnam coastal upwelling to the 1997-1998 ENSO event observed by multisensor data. Remote Sensing of Environment. 2004;**89**(1):106-115. DOI: 10.1016/j.rse.2003.10.009

[44] Yu J, Wang X, Li Y, Chen B. Analysis of the upwelling in the fishing ground in Midwestern South China Sea. Marine Sciences. 2015;**39**(6):104-113 (in Chinese)

[45] Zheng QA, Xie LL, Zheng Z-W, Hu JY. Progress in research of mesoscale eddies in the South China Sea. Advances in Marine Science. 2017;**35**(2):131-158 (in Chinese)

[46] Xie LL, Zheng QA. New insights to the South China Sea: The Rossby normal modes. Acta Oceanologic Sinica. 2017;**36**(7):1-3. DOI: 10.1007/s13131-017-1077-0

[47] Chen DK, Lei X, Wang W, Wang G, Han G, Zhou L.Upper Ocean response and feedback mechanisms to typhoon. Advances in Earth Science. 2013;**28**(10):1077-1086

[48] Zhang SW, Xie LL, Hou YJ, Zhao H, Qi YQ, Yi XF. Tropical storm-induced turbulent mixing and chlorophyll-enhancement in the continental shelf southeast of Hainan Island. Journal of Marine Systems. 2014;**129**:405-414. DOI: 10.1016/j.jmarsys.2013.09.002

[49] Dare RA, Mcbride JL. Sea surface temperature response to tropical cyclones. Monthly Weather Review. 2011;**139**:3798-3808

[50] Zheng QA, Zhu BL, Li JY, Sun ZY, Xu Y, Hu JY. Growth and dissipation of typhoon-forced solitary continental shelf waves in the northern South China Sea. Climate Dynamics. 2015;**45**(3-4):853-865. DOI: 10.1007/s00382-014-2318-y